

# MoE-FFD: Mixture of Experts for Generalized and Parameter-Efficient Face Forgery Detection

Chenqi Kong<sup>1</sup>, Anwei Luo<sup>2</sup>, Song Xia<sup>1</sup>, Yi Yu<sup>1,3</sup>, Haoliang Li<sup>4</sup>, and Alex C. Kot<sup>1</sup>

<sup>1</sup> Rapid-Rich Object Search (ROSE) Lab, School of Electrical and Electronic Engineering, Nanyang Technological University, 639798, Singapore.

<sup>2</sup> School of Computer Science and Engineering, Sun Yat-sen University, 510275, Guangzhou, China.

<sup>3</sup> Rapid-Rich Object Search (ROSE) Lab, Interdisciplinary Graduate Programme, Nanyang Technological University, 639798, Singapore.

<sup>4</sup> Department of Electrical Engineering, City University of Hong Kong, Hong Kong SAR.

{chenqi.kong, eackot}@ntu.edu.sg, luowan@mail2.sysu.edu.cn, {xias0002, yuyi0010}@e.ntu.edu.sg, haoliang.li@cityu.edu.hk

**Abstract.** Deepfakes have recently raised significant trust issues and security concerns among the public. Compared to CNN face forgery detectors, ViT-based methods take advantage of the expressivity of transformers, achieving superior detection performance. However, these approaches still exhibit the following limitations: (1). Fully fine-tuning ViT-based models from ImageNet weights demands substantial computational and storage resources; (2). ViT-based methods struggle to capture local forgery clues, leading to model bias and limited generalizability. To tackle these challenges, this work introduces Mixture-of-Experts modules for Face Forgery Detection (MoE-FFD), a generalized yet parameter-efficient ViT-based approach. MoE-FFD only updates lightweight Low-Rank Adaptation (LoRA) and Adapter layers while keeping the ViT backbone frozen, thereby achieving parameter-efficient training. Moreover, MoE-FFD leverages the expressivity of transformers and local priors of CNNs to simultaneously extract global and local forgery clues. Additionally, novel MoE modules are designed to scale the model’s capacity and select optimal forgery experts, further enhancing forgery detection performance. The proposed MoE learning scheme can be seamlessly adapted to various transformer backbones in a plug-and-play manner. Extensive experimental results demonstrate that the proposed method achieves state-of-the-art face forgery detection performance with reduced parameter overhead. The code will be released upon acceptance.

**Keywords:** Deepfakes · face forgery detection · Mixture-of-Experts · generalizability · robustness · parameter-efficient training.

## 1 Introduction

With rapid advancements in AIGC, forged face contents are becoming increasingly sophisticated. The human naked eye can hardly discriminate between fake

faces and real ones. Even non-experts can readily implement face manipulation algorithms to produce falsified facial images/videos (i.e., Deepfakes) with a high level of realism. Consequently, the rapid proliferation of Deepfake content on social media platforms has caused pressing security issues, such as disinformation, fraud, and impersonation [29]. Thus, developing accurate and robust face forgery detectors to counter malicious attacks poses a grand challenge.

Early traditional Deepfake detection methods focused on extracting hand-crafted features, such as eye-blinking frequency [37] and head-pose inconsistency [70]. These techniques fail to capture representative features because the hand-crafted features may limit their scopes to only one or few kinds of statistical information. Heading into the era of deep learning, numerous CNN-based methods have been proposed to improve the detection accuracy [11, 20, 27, 36, 42]. Many of them employ Xception network [7] or EfficientNet [63] as backbones due to their outstanding performance in face forgery detection. To enhance generalizability and robustness, some methods proposed to extract common forgery features such as noise patterns [26, 43, 45], blending artifacts [36, 58], frequency fingerprints [35, 47, 51, 68], and identity inconsistency [20], etc. However, these methods are inherently limited to the local-interactions of CNN architectures.

With the advent of the vision transformer (ViT) [13], ViT architectures have achieved significant success in various computer vision tasks due to their long-range interactions and outstanding expressivity. In the realm of Deepfake detection, numerous ViT-based approaches [12, 15, 28, 46, 55, 67, 73] have been proposed, achieving enhanced accuracy and generalizability. Nevertheless, ViT-based forgery detection approaches still face certain limitations. Firstly, fully training ViT-based models from the ImageNet weights demands substantial computational resources, hindering their deployment or fine-tuning in real-world applications, especially on mobile devices with limited processing power. Secondly, while ViT-based methods exhibit outstanding expressivity, they may struggle to capture forgery features in local abnormal regions, resulting in model bias and limited generalizability.

This paper presents a generalized yet parameter-efficient approach MoE-FFD, which proposes using **M**ixture of **E**xperts for **F**ace **F**orgery **D**etection. MoE-FFD draws inspiration from Parameter Efficient Fine-Tuning (PEFT), which integrates lightweight Low-Rank Adaptation (LoRA) layers and Adapter layers with the ViT backbone. During the training process, only the designed

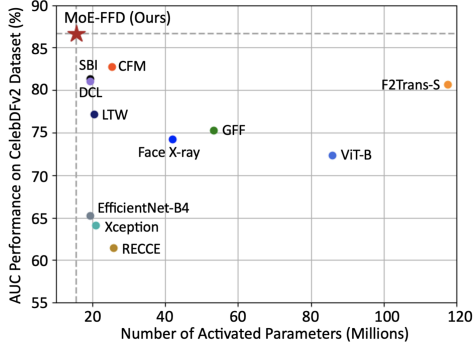


**Fig. 1:** Comparison between MoE-FFD (Ours) and Open-source face forgery detection models on the CelebDF-v2 dataset. We present the number of activated parameters and the AUC detection performance in  $x$  and  $y$  axis, respectively.

LoRA and Adapter parameters are updated while the ViT parameters remain frozen as the ImageNet weights. The designed MoE modules dynamically select optimal LoRA and Adapter experts for face forgery detection.

Compared with previous methods that directly fine-tune the entire ViT parameters, the proposed fine-tuning strategy effectively preserves abundant knowledge from ImageNet and enables the model to adaptively learn forgery-specific features. Additionally, the designed LoRA layers model the long-range interactions within input faces, while the Convpass Adapter layers effectively highlight local forgery anomalies. To this end, the integration of the designed LoRA and Adapter layers leverages the expressivity of transformers and the local forgery priors of CNNs, leading to enhanced generalizability and robustness. Moreover, we design novel MoE modules in both LoRA and Adapter layers to scale the model capacity using fixed activated parameters. MoE aims to dynamically select optimal LoRA and Adapter experts for input faces, further empowering the model’s forgery detection performance.

As depicted in Fig. 1, our MoE-FFD with the fewest activated parameters achieves the best AUC score on the unseen CelebDF-v2 dataset [39]. Overall, the contributions of this work are summarized as follows:

- We innovatively integrate LoRA and Adapter with the ViT backbone for face forgery detection. This design simultaneously mines global and local forgery clues in a more efficient manner.
- We design novel Mixture-of-Experts (MoE) modules to scale the model capacity, which dynamically select optimal forgery experts for input faces. Moreover, the designed MoE modules can be seamlessly adapted to other transformer architectures and boost the detection performance in a plug-and-play fashion.
- We conduct experiments on six Deepfake datasets and various perturbations. Extensive experimental results demonstrate that MoE-FFD achieves state-of-the-art generalizability and robustness.

## 2 Related Works

### 2.1 Face Forgery Detection

Early attempts at face forgery detection primarily relied on extracting hand-crafted features, such as the lack of eye blinking [37], inconsistency of head pose [70], face warping artifacts [38], and heart rate anomalies [8]. However, these methods suffer from limited accuracy due to their narrow focus on specific statistical information. In response, learning-based approaches have emerged, leveraging generic network architectures like Xception Network [7], EfficientNet [63], and Capsule Network [49] for forgery feature extraction. Nonetheless, CNN-based methods are prone to overfitting to the training data, resulting in limited generalizability and robustness. Follow-up works, such as Face X-ray [36], F<sup>3</sup>Net [51], SBI [59], DCL [61], and RECCE [6], have introduced comprehensive forgery frameworks and robust feature extraction techniques, enhancing the

model’s generalization capability. With the explosive development of ViT [13], numerous ViT-based methods [12, 15, 28, 46, 55, 67, 73] have been proposed to tackle the Deepfake problem. These approaches take advantage of non-inductive bias and global context understanding, achieving superior face forgery detection performance. However, most of these methods fine-tune the entire ViT model on Deepfake datasets, which is computationally expensive and may lead to loss of valuable knowledge from the ImageNet dataset [9]. In contrast, our approach finetunes external lightweight LoRA and Adapter parameters during training, keeping the ViT backbone fixed with ImageNet weights, thus enabling a parameter-efficient face forgery detection.

## 2.2 Parameter Efficient Fine-Tuning (PEFT)

Over the past few years, the size of deep learning models has exponentially increased, especially after the advent of transformers. Consequently, numerous Parameter Efficient Fine-Tuning (PEFT) methods have been proposed to reduce the computational and storage overhead. PEFT only updates a small portion of the model parameters while freezing the majority of pretrained weights. Adapter [18, 62] is a typical PEFT method, comprising a down-sample layer and an up-sample layer, generally integrated into transformer layers and blocks. Low-Rank Adaptation (LoRA) [19] layer aims at updating two low-rank matrices, significantly reducing the trainable parameters. Additionally, Visual Prompt tuning (VPT) [22] augments inputs with extra learnable tokens, which can be regarded as learnable pixels to vision transformers. Scale and Shift Feature Modulation (SSF) [40] advances further by introducing to scale and shift parameters to modulate visual features during training, achieving comparable performance compared with full fine-tuning. Convpass [24] integrates convolutional bypasses into large ViT models, leveraging local priors to improve image classification performance. However, the application of PEFT methods to face forgery detection remains largely unexplored. In this work, we incorporate dedicated forgery Adapter and LoRA layers to mine global and local clues and enhance the detection performance.

## 2.3 Mixture of Experts (MoE)

Mixture-of-Experts (MoE) [21] models aim to augment the model’s capacity without increasing computational expenses. MoE comprises multiple sub-experts and incorporates a gating mechanism to dynamically select the most relevant Top-k experts, thereby optimizing the results. The concept of MoE has been widely used in both Computer Vision [41, 48, 52, 57] and Natural Language Processing [4, 31, 56]. Sparse MoE [56] introduces a router to select a subset of experts, ensuring that the inference time is on par with the standalone counterpart. Subsequent methods such as [17, 32, 53] seek to design novel gating mechanisms to enhance the performance on specific tasks. Follow-up works [17, 30, 44] propose leveraging multi-task learning to guide the model to select optimal experts for a given input query. Moreover, some studies apply MoE architectures to domain

adaptation [16] and domain generalization [33] tasks. In our work, we draw inspiration from the concept of MoE to automate the selection of different LoRA and Adapter modules for various testing data. The designed MoE modules smartly select optimal experts and outperform previous detection methods by a clear margin.

### 3 Methods

#### 3.1 Preliminaries

**Vision Transformer** consists of multiple blocks of Self-Attention and Multi-Layer Perceptron (MLP). For a given input sequence  $x \in \mathbb{R}^{N_t \times D}$ ,  $x$  is firstly projected to queries  $Q \in \mathbb{R}^{N_t \times dim}$ , keys  $K \in \mathbb{R}^{N_t \times dim}$ , and values  $V \in \mathbb{R}^{N_t \times dim}$  using three learnable matrices  $W_q \in \mathbb{R}^{D \times dim}$ ,  $W_k \in \mathbb{R}^{D \times dim}$ , and  $W_v \in \mathbb{R}^{D \times dim}$ , where  $dim$  denotes the hidden dimension:

$$Q = xW_q, K = xW_k, V = xW_v. \quad (1)$$

Then the Self-Attention is conducted by:

$$\text{Attention}(Q, K, V) = \text{softmax}(QK^\top / \sqrt{dim})V. \quad (2)$$

**LoRA** is one popular parameter-efficient tuning method. For a pretrained ImageNet weight matrix  $W \in \mathbb{R}^{D \times dim}$ , LoRA freezes  $W$  during training while adding a product of two trainable low-rank matrices  $W^{down}W^{up}$ , where  $W^{down} \in \mathbb{R}^{D \times r}$ ,  $W^{up} \in \mathbb{R}^{r \times dim}$ , and  $\text{rank } r \ll \min(D, dim)$ . As such, the forward pass is modified as:

$$h = x(W + \Delta W) = xW + xW^{down}W^{up}. \quad (3)$$

Compared with ViT, the proposed LoRA significantly reduces the trainable parameter number.

**Convpass Adapter** integrates local priors for visual tasks, constructing Convolutional Bypasses (Convpass) within the Vision Transformer (ViT) framework as adaptation modules. The Convpass Adapter can be formulated as:

$$x_{out} = MLP(x_{in}) + Convpass(x_{in}), \quad (4)$$

where the parameters in MLP are fixed with ImageNet weights during training. Convpass generally consists of several trainable convolutional layers.

#### 3.2 Overview of the Proposed Framework

Fig. 2 illustrates the designed MoE-FFD framework. Fig. 2 (a) depicts the ViT backbone, which is initialized with the ImageNet weights. Fig. 2 (b) presents more details regarding the designed transformer blocks. We integrate the designed MoE Adapter layer and MoE LoRA layer with the vanilla ViT blocks.

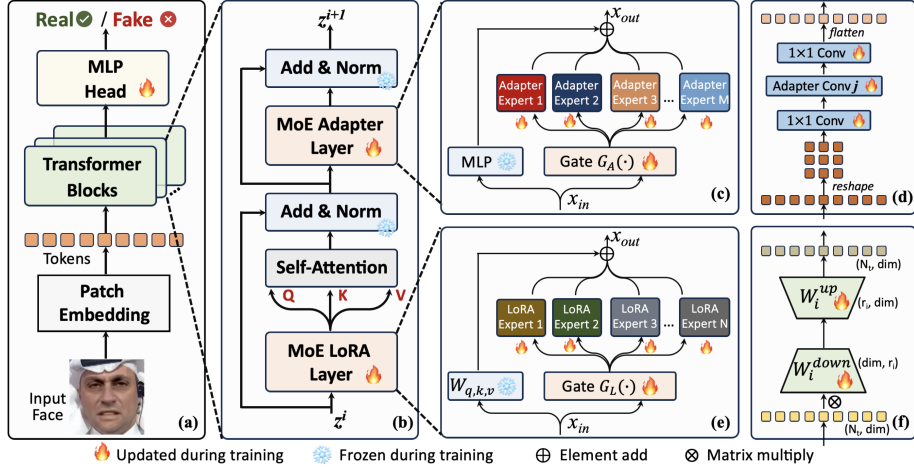


**Fig. 2:** Overview of the designed MoE-FFD framework. (a). Overall model structure; (b). Details of MoE-FFD transformer block; (c). Details of the designed MoE Adapter layer; (d). Details of each Adapter expert; (e). Details of the designed MoE LoRA layer; (f). Details of each LoRA expert.

Fig. 2 (c) details the designed MoE Adapter layer. During the training process, the MLP parameters are frozen with the ImageNet weights. Within this layer, a MoE module is designed, comprising one gate  $G_A(\cdot)$  and  $M$  forgery Adapter experts. The gating mechanism aims to dynamically select the appropriate experts for each input query, while the designed Adapter experts aim to extract specific local forgery features from the input faces. Fig. 2 (d) illustrates the structure of Adapter  $j$ . We first reshape the input feature and reduce its channel dimension by using a  $1 \times 1$  convolution. Subsequently, we design convolution operations to extract specific local forgery clues. The output feature is then passed through to another  $1 \times 1$  convolution layer to restore the channel dimension. Finally, the feature map is flattened to the original shape.

Similarly, the attention weights  $W_{q,k,v}$  in the MoE LoRA are fixed to the ImageNet weights. As shown in Fig. 2 (e), the MoE LoRA module consists of one gate  $G_L(\cdot)$  and  $N$  experts, each with a unique rank. Fig. 2 (f) depicts the LoRA structure, where  $\otimes$  indicates matrix multiplication. The output feature is derived by multiplying the input with two learnable low-rank matrices.

The whole framework is trained in an end-to-end manner with the supervision of the following objective function:

$$L = L_{ce} + \lambda \cdot L_{moe}, \quad (5)$$

where  $L_{ce}$  represents the cross-entropy loss. Following [5, 56], we further apply an additional loss  $L_{moe}$  to encourage all experts to have equal importance. Further details on  $L_{moe}$  will be dedicated at the end of this section.

### 3.3 Details of the MoE

**MoE LoRA Layer.** LoRA modules with different ranks tend to project the input tokens into various feature spaces. However, in uncontrolled deployment environments, it is challenging to manually predefine an ideal rank for different testing faces. To tackle this challenge, we design a MoE LoRA Layer that learns an optimal LoRA expert for each input query. As shown in Fig. 2 (e), each LoRA expert  $E_L(\cdot)_i$  specifies a rank  $r_i$ . In this work, we design a gating mechanism  $G_L(\cdot)$  to dynamically select the Top-k experts (default: k=1). The details of the gating mechanism will be elaborated later. As such, the output tokens can be calculated by:

$$x_{out} = W_{q/k/v}x_{in} + \sum_i^N G_L(x_{in})_i E_L(x_{in})_i, \quad (6)$$

where  $W_{q/k/v}$  is fixed as the ImageNet weight during the training process. Each LoRA expert is formulated by:

$$E_L(x_{in})_i = x_{in} W_i^{down} W_i^{up}, \quad (7)$$

where  $W_i^{up} \in \mathbb{R}^{r_i \times dim}$  and  $W_i^{down} \in \mathbb{R}^{dim \times r_i}$  are two trainable matrices.

**MoE Adapter Layer.** Previous studies [14, 55, 69] have demonstrated the effectiveness of utilizing local difference convolution to capture face forgery clues. However, these CNN-based methods only limit their scopes in one specific forgery feature. In our research, we introduce the MoE Adapter Layer integrated into the ViT backbone. This design aims to scale the model capacity and facilitate the dynamic selection of the suitable forgery Adapter expert. Additionally, the designed MoE Adapter layer dynamically injects local forgery priors into the plain ViT backbone.

As shown in Fig. 2 (c), the designed MoE Adapter layer consists of  $M$  Convpass Adapter experts. And the output  $x_{out}$  can be formularized as:

$$x_{out} = \text{MLP}(x_{in}) + \sum_j^M G_A(x_{in})_j E_A(x_{in})_j, \quad (8)$$

where MLP is frozen as the ImageNet weights during training. Adapter expert  $E_A(\cdot)_j$  can be calculated by (we omit the activation layer):

$$E_A(x_{in})_j = \text{Conv}_{1 \times 1}^{\text{up}}(\text{Conv}_{3 \times 3}^j(\text{Conv}_{1 \times 1}^{\text{down}}(x_{in}))), \quad (9)$$

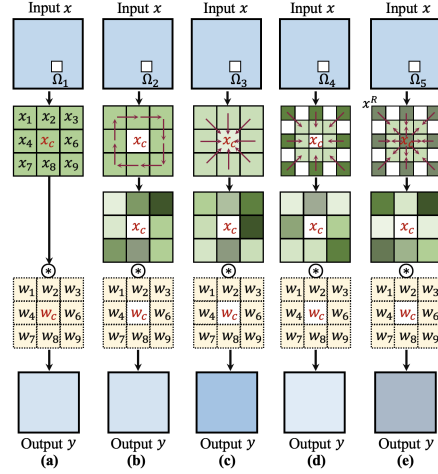


**Fig. 3:** Illustration of the designed Convpass Adapter experts.

$\text{Conv}_{1 \times 1}^{\text{down}}$  and  $\text{Conv}_{1 \times 1}^{\text{up}}$  are two  $1 \times 1$  convolution layers, which down-sample and up-sample the channels, respectively.  $\text{Conv}_{3 \times 3}^j$  indicates the specific convolution layer in different experts. We develop  $M = 5$  types of convolution. These convolutions aim to model different local interactions, facilitating the model to capture abundant local forgery features in input faces.

Fig. 3 shows the designed five convolutions, including (a). Vanilla Convolution, (b). Angular Difference Convolution (ADC), (c). Central Difference Convolution (CDC), (d). Radial Difference Convolution (RDC), and (e). Second-Order Convolution (SOC). The red arrow  $\rightarrow$  indicates the subtraction operation. We first formulate the vanilla convolution as (we omit the bias for concision):

$$y = \sum_{p \in \Omega_1} w_p x_p, \quad (10)$$

then, for the other four convolution types, Eq.(10) can be rewritten as:

$$y = \sum_{p \in \Omega_j} w_p \hat{x}_p = w_c x_c + \sum_{p \in \Omega_j, p \neq c} w_p \hat{x}_p, \quad (11)$$

where  $x_c$  and  $w_c$  represent the center elements of the input  $x$  and weight  $w$ .

In ADC and CDC, we set the  $\Omega$  size as  $3 \times 3$ . The  $\hat{x}_p$  in CDC can be calculated by:  $\hat{x}_p = x_p - x_c$ . And the  $\hat{x}_p$  in ADC is denoted as:  $\hat{x}_p = x_p - x_p^{\text{next}}$ , where  $x_p^{\text{next}}$  is the next element in the clockwise direction.

In the RDC and SOC operations, we set the size of the  $\Omega$  region as  $5 \times 5$ . For each element  $x_p$ , we define a corresponding radial element  $x_p^R$  in the peripheral region of  $\Omega$ , which is highlighted in dark green in Fig. 3 (d) and (e). As such, the  $\hat{x}_p$  in RDC is calculated by:  $\hat{x}_p = x_p^R - x_p$ . SOC aims at learning second-order local anomaly of the input. As such,  $\hat{x}_p$  in SOC is formulated as:  $\hat{x}_p = (x_p^R - x_p) - (x_p - x_c) = (x_p^R - x_p) + (x_c - x_p)$ . As such, the designed MoE Adapter layer can effectively search intrinsic detailed local forgery patterns in a larger feature space.

**Gating Network.** We adopt Top-k noisy gating [56] as our gating mechanism. The gating scores  $G(x) \in \mathbb{R}^{N_e}$  are determined by the values  $H(x) \in \mathbb{R}^{N_e}$ , where  $N_e$  indicates the expert number. For a given input  $x \in \mathbb{R}^{N_t \times \text{dim}}$ , we first apply average pooling and reshape it to  $x_m \in \mathbb{R}^{\text{dim}}$ . Then, we calculate  $H(x)$  by:

$$H(x) = x_m \otimes W_{\text{gate}} + \text{StandardNormal}()(\text{Softplus}(x_m \otimes W_{\text{noise}})), \quad (12)$$

where  $W_{\text{gate}} \in \mathbb{R}^{\text{dim} \times N_e}$  and  $W_{\text{noise}} \in \mathbb{R}^{\text{dim} \times N_e}$  are slim trainable parameters. Softplus is an activation function. For a given  $H(x) \in \mathbb{R}^{N_e}$ , we keep Top-k ( $k \leq N_e$ ) values while setting others as  $-\infty$ . Then, the gating scores  $G(x)$  can be calculated by:

$$G(x) = \text{Softmax}(\text{Topk}(H(x), k)). \quad (13)$$

To prevent the gating network from converging to a state where it produces large weights for the same few experts. We further apply a soft constraint on the



batch-wise average of each gate. As such, for a given batch of data  $X$ , the MoE loss  $L_{moe}$  is defined as:

$$L_{moe} = CV(Importance(X))^2; Importance(X) = \sum_{x \in X} G(x), \quad (14)$$

where  $CV(\cdot)$  indicates the Coefficient of Variation.

## 4 Experiments

### 4.1 Implementation Details

We apply the popular MTCNN face detector [71] to crop the face regions. The proposed framework is implemented on the Pytorch [50] platform. The model is trained using Adam optimizer [25] with  $\beta_1 = 0.9$  and  $\beta_2 = 0.999$ . We set the learning rate of gating network and other trainable parameters as  $1e-4$  and  $3e-5$ , respectively. The loss weigh  $\lambda$  in Eq. (5) is set as 1. We train the model for 20 epochs on one single 3090 GPU with batch size 32. We follow the data split strategy in [42] for fair comparison.

### 4.2 Datasets and Evaluation Metrics

The experiments encompass the following six datasets for training and testing: FaceForensics++ (FF++) [54], CelebDF-v2 (CDF) [39], WildDeepfake (WDF) [74], DeepFake Detection Challenge (DFDC) [10], DeepFakeDetection (DFD) [1], and DeepForensics-1.0 (DFR) [23]. FF++ is a widely used dataset in face forgery detection, which includes four face manipulation types: Deepfakes (DF) [2], Face2Face (FF) [65], FaceSwap (FS) [3], and NeuralTextures (NT) [64]. The remaining datasets represent recent five Deepfake datasets with diverse environment variables and various video qualities. We perform cross-dataset and cross-manipulation evaluations to examine the models' generalization capability. Additionally, we measure the model's robustness by applying it to perturbed face images with various perturbations and severity levels. Consistent with prior arts, we adopt Area under the ROC Curve (AUC) and Equal Error Rate (EER) as evaluation metrics.

### 4.3 Comparison with State-of-the-Arts

**Cross-Dataset Evaluations.** In practical scenarios, the trained models always suffer significant performance drops when tested on unseen datasets. Herein, we conduct cross-dataset experiments to evaluate the models' generalization capability. We train all models on the FF++ (C23) dataset and directly evaluate them on five unseen Deepfake datasets: CDF, WDF, DFDC, DFD, and DFR. Table 1 presents the frame-level and video-level detection results, divided into top and bottom sections. Video-level detection results are obtained by averaging all frame scores within each video. We bold the best results and underline

**Table 1:** Cross-dataset evaluation on five unseen datasets. ‘\*’ indicates the trained model provided by the authors. ‘†’ indicates our re-implementation using the public official code. Methods highlighted in blue denote video-level results. #Params indicates the activated parameter number during training.

Method	Venue	#Params	CDF		WDF		DFDC		DFD		DFR		Average	
			AUC	EER	AUC	EER	AUC	EER	AUC	EER	AUC	EER	AUC	EER
Face X-ray [36]	CVPR20	41.97M	74.20	-	-	-	70.00	-	85.60	-	-	-	-	-
GFF [43]	CVPR21	53.25M	75.31	32.48	66.51	41.52	71.58	34.77	85.51	25.64	-	-	-	-
LTW [60]	AAAI21	20.37M	77.14	29.34	67.12	39.22	74.58	33.81	88.56	20.57	-	-	-	-
F2Trans-S [46]	TIFS23	117.52M	80.72	-	-	-	71.71	-	-	-	-	-	-	-
ViT-B [13]	ICLR21	85.80M	72.35	34.50	75.29	33.40	75.58	32.11	79.61	28.85	80.47	26.97	76.66	31.17
SBI* [59]	CVPR22	19.34M	81.33	26.94	67.22	38.85	<u>79.87</u>	<u>28.26</u>	77.37	30.18	84.90	23.13	78.14	29.47
DCL* [61]	AAAI22	19.35M	81.05	26.76	72.95	35.73	71.49	35.90	89.20	19.46	92.26	14.81	81.39	26.53
Xception† [7]	ICCV19	20.81M	64.14	39.77	68.90	38.67	69.56	36.94	84.31	25.00	91.93	15.52	75.77	31.18
RECCE† [6]	CVPR22	25.83M	61.42	41.71	74.38	32.64	64.08	40.04	83.35	24.57	92.93	14.74	75.23	30.73
EN-B4† [63]	ICML19	19.34M	65.24	39.41	67.89	37.21	67.96	37.60	88.67	18.46	92.18	15.51	76.39	29.64
CFM* [42]	TIFS24	25.37M	<u>82.78</u>	<u>24.74</u>	<u>78.39</u>	<u>30.79</u>	75.82	31.67	<b>91.47</b>	<b>16.80</b>	<u>95.18</u>	<u>11.87</u>	<u>83.94</u>	<u>24.20</u>
MoE-FFD	Ours	<b>15.51M</b>	<b>86.69</b>	<b>22.06</b>	<b>80.64</b>	<b>27.11</b>	<b>80.83</b>	<b>26.67</b>	<u>90.37</u>	<u>17.67</u>	<b>95.39</b>	<b>11.29</b>	<b>86.78</b>	<b>20.96</b>
Lisiam [66]	TIFS22	-	78.21	-	-	-	-	-	-	-	-	-	-	-
F <sup>3</sup> Net [51]	ECCV20	42.53M	68.69	-	-	-	67.45	-	-	-	-	-	-	-
FTCN [72]	ICCV21	26.60M	86.90	-	-	-	74.00	-	-	-	-	-	-	-
ViT-B [13]	ICLR21	85.80M	78.12	30.59	78.95	29.59	79.43	28.62	84.52	23.48	86.42	19.90	81.49	26.44
SBI* [59]	CVPR22	19.34M	88.61	19.41	70.27	37.63	<u>84.80</u>	<u>25.00</u>	82.68	26.72	90.04	17.53	83.28	25.26
DCL* [61]	AAAI22	19.35M	88.24	19.12	76.87	31.44	77.57	29.55	<u>93.91</u>	14.40	97.41	9.96	86.80	20.89
RECCE† [6]	CVPR22	25.83M	69.25	34.38	76.99	30.49	66.90	39.39	86.87	21.55	97.15	9.29	79.42	27.01
CFM* [42]	TIFS24	25.37M	<u>89.65</u>	<u>17.65</u>	<u>82.27</u>	<u>26.80</u>	80.22	27.48	<b>95.21</b>	<b>11.98</b>	<u>97.59</u>	<u>9.04</u>	<u>88.99</u>	<u>18.59</u>
MoE-FFD	Ours	<b>15.51M</b>	<b>91.28</b>	<b>17.15</b>	<b>83.91</b>	<b>24.75</b>	<b>84.97</b>	<b>23.44</b>	93.57	<u>14.05</u>	<b>98.52</b>	<b>5.47</b>	<b>90.45</b>	<b>16.97</b>

the second-best results. Notably, MoE-FFD achieves the highest detection performance on four datasets in both frame-level and video-level detection. Additionally, MoE-FFD’s performance is on par with CFM on the DFD dataset. Moreover, MoE-FFD outperforms CFM by a clear margin in average performance. The average frame-level AUC improves by 2.86%, rising from 83.94% to 86.78%. Similarly, MoE-FFD also outperforms others in video-level detection on average.

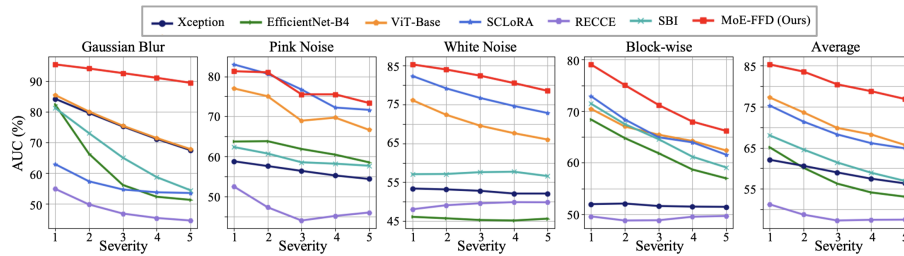
**Cross-Manipulation Evaluations.** Existing face forgery detectors are vulnerable to unforeseen manipulation types. To evaluate the generalizability to new manipulation techniques, we perform cross-manipulation experiments on four forgery techniques: Deepfakes (DF), Face2Face (FF), FaceSwap (FS), and NeuralTextures (NT). Table 2 presents the results, where models trained on three manipulation types are tested on the remaining one. MoE-FFD exhibits the best average detection results. Compared to the ViT-B baseline, the proposed method achieves an average AUC enhancement of 18.5%, going from 62.3% to 80.8%. In Table 3, we further examine models trained on one manipulation type and tested across the other three. AVG\* denotes the average AUC score across three cross-manipulation trials. MoE-FFD outperforms the baseline in both intra- and cross-manipulation evaluations. Remarkably, MoE-FFD achieves around 99% AUC scores in each intra-manipulation evaluation, highlighting its outstanding detection accuracy in intra-domain evaluations. When compared to the state-of-the-art RECCE method, our MoE-FFD consistently achieves superior average cross-manipulation results across all four evaluation settings. These findings suggest that MoE-FFD is generalized to unseen manipulations.

**Table 2:** Cross-manipulation detection AUC on the unseen manipulation method (C23).

Method	#Params	DF	FF	FS	NT	AVG
Xception [7]	20.81M	0.907	0.753	0.460	0.744	0.716
EN-B4 [63]	19.34M	0.485	0.556	0.517	0.493	0.513
AT EN-B4 [63]	19.34M	0.911	0.801	0.543	0.774	0.757
FL EN-B4 [63]	19.34M	0.903	0.798	0.503	0.759	0.741
MLDG [34]	62.38M	0.918	0.771	0.609	<b>0.780</b>	0.770
LTW [60]	20.37M	<u>0.927</u>	0.802	0.640	0.773	<u>0.786</u>
ViT-B [13]	85.80M	0.771	0.656	0.510	0.554	0.623
CFM [42]	25.37M	0.880	<u>0.814</u>	<u>0.630</u>	0.643	0.742
MoE-FFD	<b>15.51M</b>	<b>0.947</b>	<b>0.877</b>	<b>0.647</b>	<u>0.759</u>	<b>0.808</b>

**Table 3:** Cross-manipulation detection AUC on the three unseen manipulation methods (C23).

Methods	Train	DF	FF	FS	NT	AVG*
ViT [13]		99.28	59.87	49.91	62.38	57.39
RECCE [6]	DF	99.95	69.75	<b>54.72</b>	77.15	67.21
Ours		<b>99.80</b>	<b>73.46</b>	52.15	<b>77.45</b>	<b>67.69</b>
ViT [13]		74.72	99.21	57.19	56.38	62.76
RECCE [6]	FF	71.55	99.20	50.02	<b>72.27</b>	64.61
Ours		<b>86.67</b>	<b>99.43</b>	<b>66.92</b>	68.75	<b>74.11</b>
ViT [13]		78.59	61.62	99.44	46.69	62.30
RECCE [6]	FS	63.05	66.21	99.72	<b>58.07</b>	62.44
Ours		<b>79.89</b>	<b>71.45</b>	99.56	48.33	<b>66.56</b>
ViT [13]		78.46	68.31	45.07	97.19	63.95
RECCE [6]	NT	72.37	64.69	51.61	99.59	62.89
Ours		<b>80.02</b>	<b>73.02</b>	<b>51.94</b>	98.70	<b>68.33</b>

**Fig. 4:** Robustness to various common perturbations at five severity levels.

**Robustness to Real-World Perturbations.** Images and videos transmitted online always undergo various perturbations that erase forgery cues within the image/video contents. We introduce common perturbations to measure the model’s robustness: Gaussian blurring, pink noise, white noise, and blockwise. Each perturbation type includes five severity levels to simulate diverse real-world conditions. As shown in Fig. 4, the detectors’ performance consistently deteriorates with increasing severity levels. However, our proposed MoE-FFD exhibits significantly greater resilience to most perturbations compared to previous methods. Notably, MoE-FFD achieves substantial improvements in robustness compared to the ViT-B baseline.

**Discussion.** MoE-FFD achieves superior generalizability and robustness compared to previous methods, which can be attributed to the following designs: (1). MoE-FFD only updates external modules while preserving the abundant ImageNet knowledge, enabling the model to adaptively learn forgery-specific features; (2). MoE-FFD integrates the LoRA and Convpass Adapter with the ViT backbone, effectively leveraging the expressivity of transformers and the local forgery priors of CNNs; (3). The incorporation of MoE modules facilitates optimal selection of LoRA and Adapter experts for forgery feature mining. Furthermore, MoE-FFD presents a parameter-efficient approach to face forgery detection due to the utilized PEFT strategy. To validate the effectiveness of the designed components, we perform ablation experiments next.

**Table 4:** Ablation study on the designed PEFT modules.

ViT-B	MoE	MoE	CDF		DFDC		WDF	
			AUC	EER	AUC	EER	AUC	EER
✓	-	-	72.35	34.50	75.58	32.11	75.29	33.40
✓	✓	-	84.84	23.51	79.62	28.13	79.73	28.62
✓	-	✓	83.21	25.34	76.35	30.90	77.15	30.93
✓	✓	✓	<b>86.69</b>	<b>22.06</b>	<b>80.83</b>	<b>26.67</b>	<b>80.64</b>	<b>27.11</b>

**Table 6:** Impacts of the matrix rank of LoRA layers and the effectiveness of MoE.

Setting	CDF		DFDC		WDF	
	AUC	EER	AUC	EER	AUC	EER
rank=8	82.46	25.94	78.30	29.24	79.35	28.77
rank=16	82.16	26.01	77.85	29.74	79.15	29.37
rank=32	81.58	26.63	78.11	29.48	79.48	29.00
rank=48	83.10	25.06	79.06	29.45	79.50	28.92
rank=64	83.85	24.97	79.38	28.19	79.46	<b>27.99</b>
rank=96	83.50	24.86	79.53	27.69	78.28	29.14
rank=128	83.47	24.52	77.36	30.48	78.93	29.89
MoE	<b>84.84</b>	<b>23.51</b>	<b>79.62</b>	<b>28.13</b>	<b>79.73</b>	28.62

**Table 5:** Cross-dataset detection performance on different backbones.

Backbone	MoE-FFD	#Params	CDF		DFDC		WDF	
			AUC	EER	AUC	EER	AUC	EER
ViT-Tiny	-	5.52M	66.41	38.53	71.92	34.23	69.71	37.23
ViT-Tiny	✓	3.90M	76.56	31.13	73.61	32.61	75.40	31.50
ViT-Small	-	21.67M	70.03	35.71	72.19	34.02	71.67	35.66
ViT-Small	✓	7.73M	81.22	27.58	78.08	29.22	77.83	30.23
ViT-Large	-	303.30M	73.13	33.28	74.46	32.25	72.96	34.45
ViT-Large	✓	41.34M	86.21	22.11	77.51	29.45	80.00	28.33

**Table 7:** Impacts of different designed Adapters and the effectiveness of MoE.

Setting	CDF		DFDC		WDF	
	AUC	EER	AUC	EER	AUC	EER
Conv	81.25	27.36	75.01	32.39	76.28	31.15
ADC	77.52	29.86	76.41	30.99	76.48	31.45
CDC	82.50	26.12	75.66	31.66	76.06	31.21
RDC	83.05	25.39	75.12	31.90	76.16	31.86
SDC	78.29	29.54	<b>76.80</b>	30.93	76.87	31.35
MoE	<b>83.21</b>	<b>25.34</b>	76.35	<b>30.90</b>	<b>77.15</b>	<b>30.93</b>

#### 4.4 Ablation Experiments

**Impacts of the PEFT Layers.** MoE-FFD integrates one LoRA layer and one Adapter layer with each ViT block. The LoRA layer is designed to learn forgery-specific parameters for subsequent attention mechanisms, capturing long-range interactions within the input faces. Meanwhile, the Convpass Adapter introduces forgery local priors into the plain ViT model. To study the effectiveness of the designed PEFT layers, we report the cross-dataset detection results in Table 4. Utilizing MoE LoRA and MoE Adapter significantly improves detection performance across all datasets compared to the ViT-B baseline. This enhancement is attributed to the LoRA and Adapter layers effectively retaining the ImageNet knowledge while adaptively learning forgery features. Furthermore, the combination of LoRA and Adapter layers allows the model to capture both long-range interactions and local forgery cues, further enhancing its performance.

**Effectiveness on Other Backbones.** Our proposed method can be flexibly adapted to other vision transformer backbones in a plug-and-play manner. To validate this adaptability, we incorporate MoE-FFD into ViT-Tiny, ViT-Small, and ViT-Large models. The cross-dataset results are presented in Table 5. By using MoE-FFD, significant performance improvements are observed across the ViT backbones. This, in turn, demonstrates the flexibility and effectiveness of our method.

**Table 8:** MoE v.s. Multi-Experts.

Method	Training Speed	Inference Speed	CDF		DFDC		WDF	
			AUC	EER	AUC	EER	AUC	EER
Multi-E	1.67Iter/s	7.18Iter/s	85.04	23.74	80.16	27.78	78.67	30.07
MoE	<b>2.13Iter/s</b>	<b>8.82Iter/s</b>	<b>86.69</b>	<b>22.06</b>	<b>80.83</b>	<b>26.67</b>	<b>80.64</b>	<b>27.11</b>

**Table 9:** Effectiveness of loss components.

$L_{ce}$	$L_{moe}$	CDF		DFDC		WDF	
		AUC	EER	AUC	EER	AUC	EER
✓	-	82.65	25.57	78.14	29.06	76.29	30.43
✓	✓	<b>86.69</b>	<b>22.06</b>	<b>80.83</b>	<b>26.67</b>	<b>80.64</b>	<b>27.11</b>

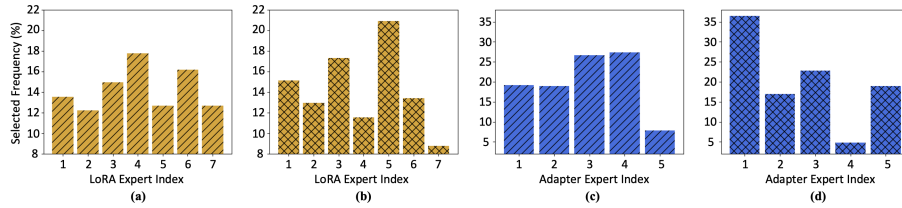


**Fig. 5:** LoRA expert selection frequency on (a). CDF and (b). WDF datasets; Adapter expert selection frequency on (c). CDF and (d). WDF datasets.

**Impacts of the MoE Learning Scheme.** The proposed MoE is designed to dynamically select the optimal experts for face forgery detection. In Table 6, we compare the performance of the proposed MoE with individual LoRA experts of varying ranks. Results show that MoE consistently outperforms individual LoRA experts on all three datasets. Notably, different datasets exhibit varying optimal LoRA ranks. Similarly, we investigate the impact of different Adapters in Table 7. Adapters tend to capture different local features of input faces. MoE again achieves the superior results compared to using a single Adapter. It should be noted that the MoE approach only introduces negligible additional activated parameters, demonstrating that the performance improvements stem from the proposed MoE learning scheme.

In Fig. 5, we further present the expert selection distributions on two datasets. Fig. 5 (a) and (b) show the LoRA expert selection frequency on CDF and WDF datasets, while Fig. 5 (c) and (d) illustrate the Adapter expert selection frequency. Different Deepfake datasets generally exhibit dramatic domain gaps. From Fig. 5, we observe distinct expert selection distributions between the CDF and WDF datasets. This finding demonstrates that MoE-FFD effectively selects the optimal experts for different data from another perspective.

**MoE v.s. Multi-Experts.** To further demonstrate the dynamic selection of optimal LoRA and Adapter experts by MoE, we compare MoE with Multi-Experts (Multi-E). Multi-E aggregates the features of all designed experts. The efficiency and the face forgery detection performance of MoE and Multi-E are reported in Table 8. Results indicate that MoE achieves a  $1.28\times$  speedup in training and  $1.23\times$  speedup in inference. Despite these efficiency gains, MoE consistently outperforms Multi-E in terms of detection performance. This observation further underscores the effectiveness of the proposed method in selecting the optimal expert for face forgery detection.

**Effectiveness of MoE Loss.** The gating network often exhibits a tendency to consistently assign large weights to only few experts [56]. To address this issue, we introduce an MoE loss component aimed at encouraging equal importance among all experts. The results in Table 9 demonstrate that  $L_{moe}$  effectively mitigates the gate overfitting problem and boosts the detection performance.

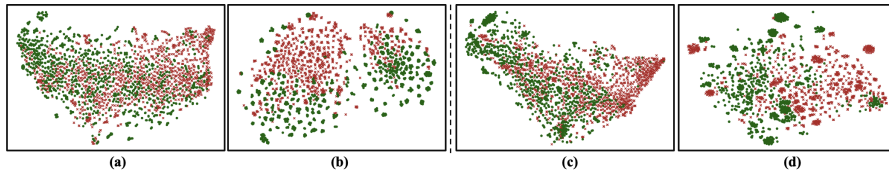


**Fig. 6:** T-SNE feature distributions of the ViT baseline and MoE-FFD. Visualization results of (a). ViT baseline on CDF dataset, (b). MoE-FFD on CDF dataset, (c). ViT baseline on WDF dataset, and (d). MoE-FFD on WDF dataset.

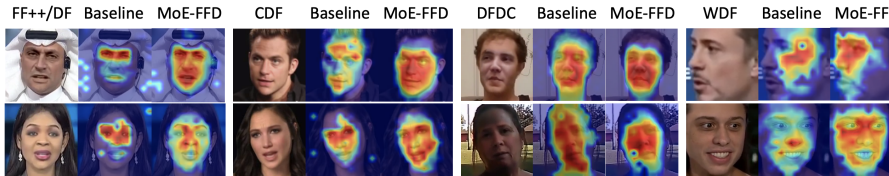


**Fig. 7:** Grad-CAM maps of the baseline model (ViT) and our proposed method MoE-FFD on four Deepfake datasets: FF++/DF, CDF, DFDC, and WDF.

#### 4.5 Visualization Results

To better demonstrate the effectiveness of our MoE-FFD method, we visualize the feature distributions of the baseline model (ViT-B) and MoE-FFD on the CDF and WDF datasets. In Fig. 6, green and red marks represent real and fake data samples, respectively. As shown in Fig. 6 (a) and (c), the baseline model struggles to discriminate the real faces from fake ones, leading to limited detection performance. In contrast, MoE-FFD feature distribution maps in Fig. 6 (b) and (d) illustrate that the real and fake faces are more discriminative.

We further provide the Grad-CAM maps of the baseline model and MoE-FFD in Fig. 7. Both models are trained on FF++ dataset and tested on four Deepfake datasets: (a). FF++/DF, (b). CDF, (c). DFDC, and (d). WDF. While the baseline model often neglects informative fake facial regions or attends to peripheral irrelevant areas, MoE-FFD consistently directs attention to manipulated regions within input face queries. This observation highlights the superiority of our method.

## 5 Conclusions

In this paper, we introduced MoE-FFD, a generalized yet parameter-efficient method for detecting face forgeries. By incorporating external lightweight LoRA and Adapter layers with the frozen ViT backbone, our framework adaptly acquired forgery-specific knowledge with minimal activated parameters. This approach not only harnesses the expressiveness of transformers but also capitalizes on the local forgery priors in CNNs, contributing to enhanced detection performance. Through dynamic expert selection within both LoRA and Adapter layers,

our MoE design further enhances the model’s generalizability and robustness. Extensive experiments consistently demonstrated MoE-FFD’s superiority in face forgery detection across diverse datasets, manipulation types, and perturbation scenarios. Moreover, MoE-FFD serves as a parameter-efficient detector and can seamlessly adapt to various ViT backbones, facilitating its deployment and fine-tuning in real-world applications. Last but not least, comprehensive ablation studies demonstrated the effectiveness of our designed LoRA layers and Conpass Adapter layers, and the MoE modules indeed helped the model to search the optimal forgery experts. We anticipate that MoE-FFD will inspire future advancements in face forgery detection, particularly in bolstering generalization and efficiency.

## References

1. <https://ai.googleblog.com/2019/09/contributing-data-to-deepfake-detection.html> 9
2. <https://github.com/deepfakes/> 9
3. <https://github.com/MarekKowalski/FaceSwap/> 9
4. Artetxe, M., Bhosale, S., Goyal, N., Mihaylov, T., Ott, M., Shleifer, S., Lin, X.V., Du, J., Iyer, S., Pasunuru, R., et al.: Efficient large scale language modeling with mixtures of experts. arXiv preprint arXiv:2112.10684 (2021) 4
5. Bengio, E., Bacon, P.L., Pineau, J., Precup, D.: Conditional computation in neural networks for faster models. arXiv preprint arXiv:1511.06297 (2015) 6
6. Cao, J., Ma, C., Yao, T., Chen, S., Ding, S., Yang, X.: End-to-end reconstruction-classification learning for face forgery detection. In: Proceedings of the IEEE/CVF Conference on Computer Vision and Pattern Recognition. pp. 4113–4122 (2022) 3, 10, 11
7. Chollet, F.: Xception: Deep learning with depthwise separable convolutions. In: Proceedings of the IEEE Conference on Computer Vision and Pattern Recognition. pp. 1251–1258 (2017) 2, 3, 10, 11
8. Ciftci, U.A., Demir, I., Yin, L.: Fakecatcher: Detection of synthetic portrait videos using biological signals. IEEE transactions on pattern analysis and machine intelligence (2020) 3
9. Deng, J., Dong, W., Socher, R., Li, L.J., Li, K., Fei-Fei, L.: Imagenet: A large-scale hierarchical image database. In: 2009 IEEE conference on computer vision and pattern recognition. pp. 248–255. Ieee (2009) 4
10. Dolhansky, B., Howes, R., Pflaum, B., Baram, N., Ferrer, C.C.: The deepfake detection challenge (dfdc) preview dataset. arXiv preprint arXiv:1910.08854 (2019) 9
11. Dong, S., Wang, J., Ji, R., Liang, J., Fan, H., Ge, Z.: Implicit identity leakage: The stumbling block to improving deepfake detection generalization. In: Proceedings of the IEEE/CVF Conference on Computer Vision and Pattern Recognition. pp. 3994–4004 (2023) 2
12. Dong, X., Bao, J., Chen, D., Zhang, T., Zhang, W., Yu, N., Chen, D., Wen, F., Guo, B.: Protecting celebrities from deepfake with identity consistency transformer. In: Proceedings of the IEEE/CVF Conference on Computer Vision and Pattern Recognition. pp. 9468–9478 (2022) 2, 4

13. Dosovitskiy, A., Beyer, L., Kolesnikov, A., Weissenborn, D., Zhai, X., Unterthiner, T., Dehghani, M., Minderer, M., Heigold, G., Gelly, S., et al.: An image is worth 16x16 words: Transformers for image recognition at scale. arXiv preprint arXiv:2010.11929 (2020) [2](#), [4](#), [10](#), [11](#)
14. Fei, J., Dai, Y., Yu, P., Shen, T., Xia, Z., Weng, J.: Learning second order local anomaly for general face forgery detection. In: Proceedings of the IEEE/CVF Conference on Computer Vision and Pattern Recognition. pp. 20270–20280 (2022) [7](#)
15. Guan, J., Zhou, H., Hong, Z., Ding, E., Wang, J., Quan, C., Zhao, Y.: Delving into sequential patches for deepfake detection. *Advances in Neural Information Processing Systems* **35**, 4517–4530 (2022) [2](#), [4](#)
16. Guo, J., Shah, D.J., Barzilay, R.: Multi-source domain adaptation with mixture of experts. arXiv preprint arXiv:1809.02256 (2018) [5](#)
17. Hazimeh, H., Zhao, Z., Chowdhery, A., Sathiamoorthy, M., Chen, Y., Mazumder, R., Hong, L., Chi, E.: Dselect-k: Differentiable selection in the mixture of experts with applications to multi-task learning. *Advances in Neural Information Processing Systems* **34**, 29335–29347 (2021) [4](#)
18. Houlsby, N., Giurgiu, A., Jastrzebski, S., Morrone, B., De Laroussilhe, Q., Gesmundo, A., Attariyan, M., Gelly, S.: Parameter-efficient transfer learning for nlp. In: International Conference on Machine Learning. pp. 2790–2799. PMLR (2019) [4](#)
19. Hu, E.J., Shen, Y., Wallis, P., Allen-Zhu, Z., Li, Y., Wang, S., Wang, L., Chen, W.: Lora: Low-rank adaptation of large language models. arXiv preprint arXiv:2106.09685 (2021) [4](#)
20. Huang, B., Wang, Z., Yang, J., Ai, J., Zou, Q., Wang, Q., Ye, D.: Implicit identity driven deepfake face swapping detection. In: Proceedings of the IEEE/CVF Conference on Computer Vision and Pattern Recognition. pp. 4490–4499 (2023) [2](#)
21. Jacobs, R.A., Jordan, M.I., Nowlan, S.J., Hinton, G.E.: Adaptive mixtures of local experts. *Neural computation* **3**(1), 79–87 (1991) [4](#)
22. Jia, M., Tang, L., Chen, B.C., Cardie, C., Belongie, S., Hariharan, B., Lim, S.N.: Visual prompt tuning. In: European Conference on Computer Vision. pp. 709–727. Springer (2022) [4](#)
23. Jiang, L., Li, R., Wu, W., Qian, C., Loy, C.C.: Deepforensics-1.0: A large-scale dataset for real-world face forgery detection. In: Proceedings of the IEEE/CVF Conference on Computer Vision and Pattern Recognition. pp. 2889–2898 (2020) [9](#)
24. Jie, S., Deng, Z.H.: Convolutional bypasses are better vision transformer adapters. arXiv preprint arXiv:2207.07039 (2022) [4](#)
25. Kingma, D.P., Ba, J.: Adam: A method for stochastic optimization. arXiv preprint arXiv:1412.6980 (2014) [9](#)
26. Kong, C., Chen, B., Li, H., Wang, S., Rocha, A., Kwong, S.: Detect and locate: Exposing face manipulation by semantic-and noise-level telltales. *IEEE Transactions on Information Forensics and Security* **17**, 1741–1756 (2022) [2](#)
27. Kong, C., Chen, B., Yang, W., Li, H., Chen, P., Wang, S.: Appearance matters, so does audio: Revealing the hidden face via cross-modality transfer. *IEEE Transactions on Circuits and Systems for Video Technology* **32**(1), 423–436 (2021) [2](#)
28. Kong, C., Li, H., Wang, S.: Enhancing general face forgery detection via vision transformer with low-rank adaptation. arXiv preprint arXiv:2303.00917 (2023) [2](#), [4](#)
29. Kong, C., Wang, S., Li, H.: Digital and physical face attacks: Reviewing and one step further. arXiv preprint arXiv:2209.14692 (2022) [2](#)



30. Kudugunta, S., Huang, Y., Bapna, A., Krikun, M., Lepikhin, D., Luong, M.T., Firat, O.: Beyond distillation: Task-level mixture-of-experts for efficient inference. arXiv preprint arXiv:2110.03742 (2021) [4](#)
31. Lepikhin, D., Lee, H., Xu, Y., Chen, D., Firat, O., Huang, Y., Krikun, M., Shazeer, N., Chen, Z.: Gshard: Scaling giant models with conditional computation and automatic sharding. arXiv preprint arXiv:2006.16668 (2020) [4](#)
32. Lewis, M., Bhosale, S., Dettmers, T., Goyal, N., Zettlemoyer, L.: Base layers: Simplifying training of large, sparse models. In: International Conference on Machine Learning. pp. 6265–6274. PMLR (2021) [4](#)
33. Li, B., Shen, Y., Yang, J., Wang, Y., Ren, J., Che, T., Zhang, J., Liu, Z.: Sparse mixture-of-experts are domain generalizable learners. arXiv preprint arXiv:2206.04046 (2022) [5](#)
34. Li, D., Yang, Y., Song, Y.Z., Hospedales, T.: Learning to generalize: Meta-learning for domain generalization. In: Proceedings of the AAAI conference on artificial intelligence. vol. 32 (2018) [11](#)
35. Li, J., Xie, H., Li, J., Wang, Z., Zhang, Y.: Frequency-aware discriminative feature learning supervised by single-center loss for face forgery detection. In: Proceedings of the IEEE/CVF Conference on Computer Vision and Pattern Recognition. pp. 6458–6467 (2021) [2](#)
36. Li, L., Bao, J., Zhang, T., Yang, H., Chen, D., Wen, F., Guo, B.: Face x-ray for more general face forgery detection. In: Proceedings of the IEEE/CVF conference on computer vision and pattern recognition. pp. 5001–5010 (2020) [2](#), [3](#), [10](#)
37. Li, Y., Chang, M.C., Lyu, S.: In ictu oculi: Exposing ai created fake videos by detecting eye blinking. In: 2018 IEEE International Workshop on Information Forensics and Security (WIFS). pp. 1–7. IEEE (2018) [2](#), [3](#)
38. Li, Y., Lyu, S.: Exposing deepfake videos by detecting face warping artifacts. arXiv preprint arXiv:1811.00656 (2018) [3](#)
39. Li, Y., Yang, X., Sun, P., Qi, H., Lyu, S.: Celeb-df: A large-scale challenging dataset for deepfake forensics. In: Proceedings of the IEEE/CVF Conference on Computer Vision and Pattern Recognition. pp. 3207–3216 (2020) [3](#), [9](#)
40. Lian, D., Zhou, D., Feng, J., Wang, X.: Scaling & shifting your features: A new baseline for efficient model tuning. *Advances in Neural Information Processing Systems* **35**, 109–123 (2022) [4](#)
41. Lou, Y., Xue, F., Zheng, Z., You, Y.: Cross-token modeling with conditional computation. arXiv preprint arXiv:2109.02008 (2021) [4](#)
42. Luo, A., Kong, C., Huang, J., Hu, Y., Kang, X., Kot, A.C.: Beyond the prior forgery knowledge: Mining critical clues for general face forgery detection. *IEEE Transactions on Information Forensics and Security* **19**, 1168–1182 (2024). <https://doi.org/10.1109/TIFS.2023.3332218> [2](#), [9](#), [10](#), [11](#)
43. Luo, Y., Zhang, Y., Yan, J., Liu, W.: Generalizing face forgery detection with high-frequency features. In: Proceedings of the IEEE/CVF Conference on Computer Vision and Pattern Recognition. pp. 16317–16326 (2021) [2](#), [10](#)
44. Ma, J., Zhao, Z., Yi, X., Chen, J., Hong, L., Chi, E.H.: Modeling task relationships in multi-task learning with multi-gate mixture-of-experts. In: Proceedings of the 24th ACM SIGKDD international conference on knowledge discovery & data mining. pp. 1930–1939 (2018) [4](#)
45. Masi, I., Killekar, A., Mascarenhas, R.M., Gurudatt, S.P., AbdAlmageed, W.: Two-branch recurrent network for isolating deepfakes in videos. In: European Conference on Computer Vision. pp. 667–684. Springer (2020) [2](#)

46. Miao, C., Tan, Z., Chu, Q., Liu, H., Hu, H., Yu, N.: F2trans: High-frequency fine-grained transformer for face forgery detection. *IEEE Transactions on Information Forensics and Security* **18**, 1039–1051 (2023) [2](#), [4](#), [10](#)
47. Miao, C., Tan, Z., Chu, Q., Yu, N., Guo, G.: Hierarchical frequency-assisted interactive networks for face manipulation detection. *IEEE Transactions on Information Forensics and Security* **17**, 3008–3021 (2022) [2](#)
48. Mustafa, B., Riquelme, C., Puigcerver, J., Jenatton, R., Houlsby, N.: Multimodal contrastive learning with limoe: the language-image mixture of experts. *Advances in Neural Information Processing Systems* **35**, 9564–9576 (2022) [4](#)
49. Nguyen, H.H., Yamagishi, J., Echizen, I.: Capsule-forensics: Using capsule networks to detect forged images and videos. In: *ICASSP 2019-2019 IEEE International Conference on Acoustics, Speech and Signal Processing (ICASSP)*. pp. 2307–2311. IEEE (2019) [3](#)
50. Paszke, A., Gross, S., Massa, F., Lerer, A., Bradbury, J., Chanan, G., Killeen, T., Lin, Z., Gimelshein, N., Antiga, L., et al.: Pytorch: An imperative style, high-performance deep learning library. *Advances in neural information processing systems* **32** (2019) [9](#)
51. Qian, Y., Yin, G., Sheng, L., Chen, Z., Shao, J.: Thinking in frequency: Face forgery detection by mining frequency-aware clues. In: *European Conference on Computer Vision*. pp. 86–103. Springer (2020) [2](#), [3](#), [10](#)
52. Riquelme, C., Puigcerver, J., Mustafa, B., Neumann, M., Jenatton, R., Susano Pinto, A., Keyzers, D., Houlsby, N.: Scaling vision with sparse mixture of experts. *Advances in Neural Information Processing Systems* **34**, 8583–8595 (2021) [4](#)
53. Roller, S., Sukhbaatar, S., Weston, J., et al.: Hash layers for large sparse models. *Advances in Neural Information Processing Systems* **34**, 17555–17566 (2021) [4](#)
54. Rossler, A., Cozzolino, D., Verdoliva, L., Riess, C., Thies, J., Nießner, M.: Face-forensics++: Learning to detect manipulated facial images. In: *Proceedings of the IEEE/CVF International Conference on Computer Vision*. pp. 1–11 (2019) [9](#)
55. Shao, R., Wu, T., Liu, Z.: Detecting and recovering sequential deepfake manipulation. In: *European Conference on Computer Vision*. pp. 712–728. Springer (2022) [2](#), [4](#), [7](#)
56. Shazeer, N., Mirhoseini, A., Maziarz, K., Davis, A., Le, Q., Hinton, G., Dean, J.: Outrageously large neural networks: The sparsely-gated mixture-of-experts layer. *arXiv preprint arXiv:1701.06538* (2017) [4](#), [6](#), [8](#), [13](#)
57. Shen, S., Yao, Z., Li, C., Darrell, T., Keutzer, K., He, Y.: Scaling vision-language models with sparse mixture of experts. *arXiv preprint arXiv:2303.07226* (2023) [4](#)
58. Shi, B., Zhang, D., Dai, Q., Zhu, Z., Mu, Y., Wang, J.: Informative dropout for robust representation learning: A shape-bias perspective. In: *International Conference on Machine Learning*. pp. 8828–8839. PMLR (2020) [2](#)
59. Shiohara, K., Yamasaki, T.: Detecting deepfakes with self-blended images. In: *Proceedings of the IEEE/CVF Conference on Computer Vision and Pattern Recognition*. pp. 18720–18729 (2022) [3](#), [10](#)
60. Sun, K., Liu, H., Ye, Q., Gao, Y., Liu, J., Shao, L., Ji, R.: Domain general face forgery detection by learning to weight. In: *Proceedings of the AAAI conference on Artificial Intelligence*. vol. 35, pp. 2638–2646 (2021) [10](#), [11](#)
61. Sun, K., Yao, T., Chen, S., Ding, S., Li, J., Ji, R.: Dual contrastive learning for general face forgery detection. In: *Proceedings of the AAAI Conference on Artificial Intelligence*. vol. 36, pp. 2316–2324 (2022) [3](#), [10](#)

62. Sung, Y.L., Cho, J., Bansal, M.: Lst: Ladder side-tuning for parameter and memory efficient transfer learning. *Advances in Neural Information Processing Systems* **35**, 12991–13005 (2022) [4](#)
63. Tan, M., Le, Q.: Efficientnet: Rethinking model scaling for convolutional neural networks. In: *International Conference on Machine Learning*. pp. 6105–6114. PMLR (2019) [2](#), [3](#), [10](#), [11](#)
64. Thies, J., Zollhöfer, M., Nießner, M.: Deferred neural rendering: Image synthesis using neural textures. *Acm Transactions on Graphics (TOG)* **38**(4), 1–12 (2019) [9](#)
65. Thies, J., Zollhofer, M., Stamminger, M., Theobalt, C., Nießner, M.: Face2face: Real-time face capture and reenactment of rgb videos. In: *Proceedings of the IEEE conference on computer vision and pattern recognition*. pp. 2387–2395 (2016) [9](#)
66. Wang, J., Sun, Y., Tang, J.: Lisiam: Localization invariance siamese network for deepfake detection. *IEEE Transactions on Information Forensics and Security* **17**, 2425–2436 (2022) [10](#)
67. Wang, J., Wu, Z., Ouyang, W., Han, X., Chen, J., Jiang, Y.G., Li, S.N.: M2tr: Multi-modal multi-scale transformers for deepfake detection. In: *Proceedings of the 2022 international conference on multimedia retrieval*. pp. 615–623 (2022) [2](#), [4](#)
68. Xu, K., Qin, M., Sun, F., Wang, Y., Chen, Y.K., Ren, F.: Learning in the frequency domain. In: *Proceedings of the IEEE/CVF Conference on Computer Vision and Pattern Recognition*. pp. 1740–1749 (2020) [2](#)
69. Yang, J., Li, A., Xiao, S., Lu, W., Gao, X.: Mtd-net: learning to detect deep-fakes images by multi-scale texture difference. *IEEE Transactions on Information Forensics and Security* **16**, 4234–4245 (2021) [7](#)
70. Yang, X., Li, Y., Lyu, S.: Exposing deep fakes using inconsistent head poses. In: *ICASSP 2019-2019 IEEE International Conference on Acoustics, Speech and Signal Processing (ICASSP)*. pp. 8261–8265. IEEE (2019) [2](#), [3](#)
71. Zhang, K., Zhang, Z., Li, Z., Qiao, Y.: Joint face detection and alignment using multitask cascaded convolutional networks. *IEEE signal processing letters* **23**(10), 1499–1503 (2016) [9](#)
72. Zheng, Y., Bao, J., Chen, D., Zeng, M., Wen, F.: Exploring temporal coherence for more general video face forgery detection. In: *Proceedings of the IEEE/CVF international conference on computer vision*. pp. 15044–15054 (2021) [10](#)
73. Zhuang, W., Chu, Q., Tan, Z., Liu, Q., Yuan, H., Miao, C., Luo, Z., Yu, N.: Uia-vit: Unsupervised inconsistency-aware method based on vision transformer for face forgery detection. In: *European Conference on Computer Vision*. pp. 391–407. Springer (2022) [2](#), [4](#)
74. Zi, B., Chang, M., Chen, J., Ma, X., Jiang, Y.G.: Wilddeepfake: A challenging real-world dataset for deepfake detection. In: *Proceedings of the 28th ACM International Conference on Multimedia*. pp. 2382–2390 (2020) [9](#)